Scientific Research Publishing

Open Journal of Fluid Dynamics, 2022, 12, 304-320
https://www.scirp.org/journal/ojfd
ISSN Online: 2165-3860
ISSN Print: 2165-3852

Mathematical Formulation of Bubble Formation after Compressible Boundary Layer Separation: Preliminary Numerical Results

Michail A. Xenos

Section of Applied and Computational Mathematics, Department of Mathematics, University of Ioannina, Ioannina, Greece
Email: mxenos@uoi.gr

How to cite this paper: Xenos, M.A. (2022) Mathematical Formulation of Bubble Formation after Compressible Boundary Layer Separation: Preliminary Numerical Results. *Open Journal of Fluid Dynamics*, **12**, 304-320.
https://doi.org/10.4236/ojfd.2022.124015

Received: October 12, 2022
Accepted: December 12, 2022
Published: December 15, 2022

Abstract

Laminar boundary layer (BL), under adverse pressure gradient, can separate. The separated shear layer reattaches to form a laminar separation bubble. Such bubbles are usually observed on gas turbine blades, on low Reynolds number wings and close to the leading edges of airfoils. Presence of bubbles has a weakening effect on the performance of a fluid device. The understanding of the prevailing mechanism of the separation bubble and ways to control it are essential for the efficient design of these devices. This is due to the significance of drag reduction in these various aerodynamic devices, such as gas turbines, re-entry space vehicles and airfoils. This study introduces a two-dimensional mathematical formulation of bubble formation after flow separation. The laminar BL equations with appropriate boundary conditions are dimensionalized using the Falkner-Skan transformation. Additionally, using the Keller-box method, the nonlinear system of partial differential equations (PDEs) is numerically solved. This study presents preliminary numerical results of bubble formation in low Mach numbers. These results reveal that after separation, a laminar bubble is formed in all studied cases, for Mach numbers, $M = 0.2$, 0.33 and 1.0. The flow after separation reverses close to the wall and finally reattaches downstream, in a new location. As the Mach number increases, this effect is more intense. After reattachment, the BL is again established in a lower energy level and the velocity field is substantially reduced, for all cases.

Keywords

Laminar Separation Bubble, Compressible Boundary Layer, Fluid Mechanics, Computational Fluid Dynamics

1. Introduction

Laminar boundary layer (BL) is highly influenced by an adverse pressure gradient. This pressure gradient could lead to flow separation causing undesired effects. As a countermeasure of flow separation, the idea of controlling the BL flow is introduced. Many researchers have proposed several control techniques to retain flow separation.

Controlling flow separation. Methods for controlling fluid flow separation by electromagnetic forces date to the 60s. One of the first who studied the incompressible BL flow over a flat plate in the presence of a uniform magnetic field, normal to the plate, was Rossow [1]. Additionally, Bleviss studied the magnetohydrodynamic (MHD) effects on hypersonic flow under the influence of a uniform magnetic field, imposed normal to the wall [2]. Recently, the influence of a magnetic field on the BL flow has attracted attention as a control technique [3]. The magnetic field can delay flow transition from laminar to turbulent. It can also delay the turbulent BL separation. The gas (air) can become weakly ionized either by viscous heating at high temperatures or by artificially generated plasma at lower temperatures, especially in high Mach number flows [3].

Another approach for controlling BL flow is the thermal radiation. The radiation effect is more noticeable at high temperatures providing important engineering applications [4] [5] [6]. The study of compressible and turbulent BL flow under the influence of thermal radiation and adverse pressure gradient has received little attention [3]. A computational model for convective and radiative heat transfer in high temperature nuclear reactors was introduced by Anghaie and Chen. This computational model considers the turbulent compressible flow under the radiation effect in a large temperature range [7]. The emission turbulence-radiation interaction in hypersonic BLs was studied by Duan *et al.* [8] [9]. In this case, when emission is introduced to the flow, the temperature is significantly decreased in the turbulent BL. A numerical analysis of heat transfer, natural convection, conduction, and thermal radiation in a rectangular domain was performed by Miroshnichenko *et al.* [10] [11]. The compressible turbulent flow over a backward facing step was studied by Kim and Baek. The study shows that thermal behavior is significantly influenced by radiation [12].

Türkyılmazoglu *et al.* studied the absolute/convective instability of two-dimensional wakes that are formed behind a flat plate, near the trailing-edge of a thin wedge-shaped airfoil in an incompressible/compressible fluid [13]. In this study, solving numerically the classical compressible BL equations with an adverse pressure gradient, the mean velocity profiles were obtained. A linear stability analysis of the BL showed that a pocket of absolute instability occurs downstream of the trailing-edge. This instability region is increasing with more adverse pressure gradients. In a similar study, Turkyilmazoglu explored the nature of the flow in the vicinity of the trailing edge of Joukowski-type airfoil configurations using the asymptotic interactive BL theory and employing a spectral numerical scheme [14]. The analysis showed that flow separation always takes place beyond a certain critical value of the thickness-to-chord ratio parameter, under the effect of a self-induced pressure gradient. Additionally, reversed flow regions of a sufficiently large size are found to be unstable. In a third study, the asymptotic theory of flow separation is used to derive the interactive BL equations governing the flow motion in the vicinity of the trailing edge of thin airfoil shapes, whose trailing edge is represented in a mathematical form, $y(x) = \alpha(-x)^m$. The analysis showed that flow separation always takes place beyond a critical value of the parameter, α, under the action of a self-induced pressure gradient. The critical value is found to be coincident for each m, with the one related to the wedged trailing edge [15].

Additionally, to prevent flow separation suction and/or injection have often been used as an active aerodynamic flow control technique. The combination of suction and injection is one of the most effective approaches for BL control [16]. The response of the turbulent or laminar BL under localized wall suction/injection and suction throughout the wall was studied by several researchers [17] [18] [19]. The combined effect of localized injection/suction retains BL flow, reducing significantly skin friction [18]. Another mean of BL control is heating and/or cooling of the wall [20].

An adverse pressure gradient could lead to separation of the laminar BL very close to the leading edge of the airfoil. The separated shear layer further reattaches on the surface to form a "laminar separation bubble". These bubbles are usually observed on gas turbine blades and on low Reynolds number wings, close to the leading edges of the airfoils [21]. When appear, separation bubbles have a deteriorating effect on the device performance. To efficient design aerodynamic devices, it is important to understand the prevailing mechanism of the laminar separation bubble and ways to control it. This could lead to drag reduction in these various aerodynamic devices.

Laminar separation bubbles. At low Reynolds numbers, the performance of the aerodynamic devices is strongly influenced by laminar separation bubbles. As mentioned before, such a separation bubble is usually appearing due to a strong pressure increase along the aerodynamic surface. This pressure increase is related to significant velocity drop towards the trailing edge of the airfoil, leading to separation of the laminar BL from the airfoil [21].

The separated, laminar flow is highly sensitive to any disturbance and quickly transitions to the turbulent state. The transition region is located at the outer BL of the separated area. The thickness of the turbulent BL rapidly grows and forms a turbulent wedge, which may eventually reach the airfoil surface. The region where the turbulent flow reaches again the surface is called the "reattachment point". So, we can provide the definition of the laminar separation bubble, where is the volume enclosed by the regions of separated laminar flow and the reattached turbulent flow. In the laminar separation bubble, the flow is circulating with almost no energy exchange with the outer flow, which makes the laminar separation bubble a stable structure [21] [22]. The laminar separation bubble significantly increases the drag of the airfoil and the BL thickness. This drag increment could be several times the drag of the airfoil with a healthy flow, meaning a flow without a separation bubble. To that extent, stability and control of an aerodynamic device can be influenced substantially by a laminar separation bubble [21] [22].

Complete BL flow separation. When transition occurs very far away from the airfoil, the turbulent flow wedge cannot reach the surface. In this case, there is no reattachment, and the bubble remains open. Such a flow field, which is composed of a thick area of separated flow, retains high drag values and lift breaks down, leading to stall effects. This phenomenon is similar to what happens when the angle of attack, α, is increased beyond the maximum lift angle [21] [22] [23].

Means to avoid separation bubbles in the BL. An effective way to avoid BL separation caused by laminar bubbles, are the "vortex generators" [24]. These are devices used to delay flow separation. To accomplish this, vortex generators are placed on external surfaces of vehicles and blades. They are usually installed close to the airfoil's leading edge, maintaining steady flow over the surface near the trailing edge of the airfoil. Vortex generators are typically rectangular or triangular. Their height is about the thickness of the local BL and they are placed in lines near the thickest part of the airfoil [24].

Mathematical modeling of laminar separation bubble. Initially, scientists believed that BL mathematical theory was not sufficient to describe separated flows and regions of reverse flow. Goldstein showed that the solution of the classical BL formulation has a singularity at the separation point. However, Catherall and Mangler were able to compute a smooth solution beyond the separation point. To achieve that, they replaced the classical formulation by a new one, where the displacement thickness, δ^*, is specified. To that extent, the external flow velocity, or equivalently the downstream pressure gradient, is not specified [25].

In this study, a two-dimensional mathematical formulation of bubble formation after flow separation is introduced. The laminar BL equations with boundary conditions, where displacement thickness is specified, δ^*, (non-classical formulation), are transformed using the Falkner-Skan transformation. The system of nonlinear and coupled partial differential equations (PDEs) is numerically solved using the Keller-box method. This study presents preliminary numerical results of bubble formation in low Mach numbers.

2. Mathematical Formulation

When a laminar BL encounters an adverse pressure gradient the flow usually separates, leading to the formation of a laminar separation bubble. Downstream of the separation point, defined as x_S in **Figure 1**, the flow is divided into two regions [22]. The first region, close to the flat plate, represents the recirculatory flow forming a laminar separation bubble, **Figure 1**. The second flow region consists of a shear layer enclosed between the outer edge of the BL and the separation bubble. Eventually, due to momentum transfer between the two regions the reverse flow eliminates near the wall and the flow reattaches at point x_R, **Figure 1**. This process composed of separation, transition, and reattachment,

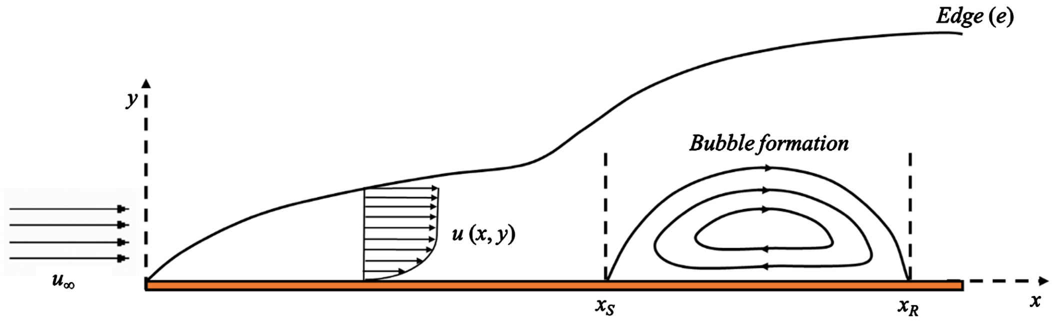

Figure 1. Problem description for laminar flow, separation of the BL and laminar separation bubble (LSB) formation, x_S is the location of BL separation, x_R is the reattachment location.

leads in the formation of a laminar separation bubble. This bubble has a dominant and undesired effect on the entire flow field. In this process, the viscous damping effect increases, and it tends to suppress the transition or to delay the BL reattachment, as the Reynolds number decreases [21] [22] [23]. In this case is difficult to obtain the edge velocity, $u = u_e(x)$, or the pressure, $p = p(x)$. So, we specify the displacement thickness of the BL, defined for a compressible flow as, $\delta^*(x) = \int_0^{y_e}\left(1 - \frac{\rho u}{\rho_e u_e}\right)\mathrm{d}y$ [25].

2.1. Mathematical Formulation Bubble Formation—Inverse BL Problems

The problem under consideration can be described by the continuity and the momentum PDEs, Equations (1)-(3), and for a compressible fluid are [17] [20],

$$\frac{\partial}{\partial x}(\rho u) + \frac{\partial}{\partial y}(\rho v) = 0, \tag{1}$$

$$\rho u \frac{\partial u}{\partial x} + \rho v \frac{\partial u}{\partial y} = -\frac{\partial p}{\partial x} + \frac{\partial}{\partial y}\left(\mu \frac{\partial u}{\partial y}\right), \tag{2}$$

$$\frac{\partial p}{\partial y} = 0, \tag{3}$$

with the following boundary conditions are,

$$\begin{aligned} &y = 0: \quad u(x,0) = v(x,0) = 0, \\ &y = y_e: \quad \delta^*(x) = \int_0^{y_e}\left(1 - \frac{\rho u}{\rho_e u_e}\right)\mathrm{d}y, \end{aligned} \tag{4}$$

where, $\delta^*(x)$ is the displacement thickness. This approach is called inverse BL problem formulation and is introduced for reverse flow calculations [25]. In the inverse problem formulation, we specify the displacement thickness $\delta^*(x)$, rather specifying the edge velocity, $u = u_e(x)$, or the pressure, $p = p(x)$ (classical boundary layer formulation). When the *u*-velocity becomes negative is common to such computations to drop the convective terms, uu_x. We then correct this approximation with upstream-downstream iterations. Introducing the following transformation,

$$\eta = \int_0^y \left(\frac{\rho_e u_e}{\mu_e x}\right)^{1/2} \frac{\rho}{\rho_e} \mathrm{d}y, \quad \psi(x,y) = (\rho_e \mu_e u_e x)^{1/2} f(x,\eta), \tag{5}$$

where η, is the dimensionless distance normal to the wall, and the stream function, ψ, for a compressible flow, we obtain the dimensionalized set of equations. The above equation, Equation (5), identically satisfies the continuity Equation (1), by the relations,

$$\rho u = \frac{\partial \psi}{\partial y}, \quad \rho v = -\frac{\partial \psi}{\partial x}. \tag{6}$$

The momentum equation is transformed to the following,

$$(bf'')' + m_1 f f'' + m_2\left[c - (f')^2\right] = x\left(f'\frac{\partial f'}{\partial x} - f''\frac{\partial f}{\partial x}\right), \tag{7}$$

where b, c, m_1 and m_2 are given as,

$$\begin{gathered} m_1 = \frac{1}{2}\left[1 + m_2 + \frac{x}{\rho_e \mu_e}\frac{\mathrm{d}}{\mathrm{d}x}(\rho_e \mu_e)\right], \quad m_2 = \frac{x}{u_e}\frac{\mathrm{d}u_e}{\mathrm{d}x}, \\ b = \frac{\rho\mu}{\rho_e \mu_e}, \quad c = \frac{\rho_e}{\rho}, \quad R_x = \frac{\rho_e u_e x}{\mu_e}, \end{gathered} \tag{8}$$

where R_x is the local Reynolds number. Additionally, we evaluate the Mach number, $M = \frac{u}{u_s}$, where u_s is the speed of sound, and the velocity, $u_e = u_e(x)$, is an unknown function of x, describing the adverse pressure gradient imposed to the boundary layer flow. Where the prime denotes partial differentiation in respect to η, ($f' = \frac{\partial f}{\partial \eta}$). The following boundary conditions are transformed to,

$$\begin{aligned} &\eta = 0: \quad f = f' = 0, \\ &\eta = \eta_e: \quad f = \frac{f'_{\eta_e}}{\rho_e}\left(\int_0^{\eta_e} f'(\eta)\,\mathrm{d}\eta - c\right), \end{aligned} \tag{9}$$

where $f'(\eta)$, is the unknown dimensionless velocity, also evaluated at the BL edge, f'_{η_e}, ρ_e, is the edge density and c is a positive constant ($c \ge 0$) defined in the literature from experimental data [25]. Equations (7)-(9) provide a new formulation for the evaluation of the bubble formation. This description is different from the classical boundary layer formulation and can effectively evaluate the bubble occurring after the separation point [25].

2.2. Evaluation of Initial Data—Classical Boundary Layer Problem

To compute bubble formation, the inverse problem, Equations (7)-(9), requires the evaluation of the flow field at an upstream location. To obtain the flow field we utilize the classical boundary layer formulation. In previous studies, we evaluate the boundary layer until the point of separation, $x = x_s$ [17]. Following a similar approach, described in the previous section, we evaluate the flow field just before the point of separation, using the classical BL formulation. The pressure gradient is expressed as a function of the edge velocity, using the Bernoulli's equation [17]. Introducing the energy equation in the formulation written as,

$$\rho u\frac{\partial H}{\partial x}+\rho v\frac{\partial H}{\partial y}=\frac{\partial}{\partial y}\left[\frac{\mu}{Pr}\frac{\partial H}{\partial y}+\mu\left(1-\frac{1}{Pr}\right)u\frac{\partial u}{\partial y}\right], \tag{10}$$

where H is the fluid's total enthalpy defined for a perfect gas (air) by the expression, $H=c_pT+u^2/2$ and $Pr=\mu c_p/k$ is the Prandtl number, we can evaluate the temperature in the BL until the point of separation, $x = x_s$, where c_p, k are constants [17].

Introducing in Equations (1)-(3) the Falkner-Skan transformation, Equation (5), and the stream function, ψ, for a compressible flow, continuity is satisfied. Additionally, if $S = H/H_e$, where H_e is the enthalpy at the BL edge, the momentum and energy equations become,

$$\left(bf''\right)'+m_1 f f''+m_2\left[c-\left(f'\right)^2\right]=x\left(f'\frac{\partial f'}{\partial x}-f''\frac{\partial f}{\partial x}\right), \tag{11}$$

$$\left(eS'+df'f''\right)'+m_1 f S'=x\left(f'\frac{\partial S}{\partial x}-S'\frac{\partial f}{\partial x}\right), \tag{12}$$

where b, c, d, e, m_1 and m_2 are given similarly as,

$$\begin{gathered}m_1=\frac{1}{2}\left[1+m_2+\frac{x}{\rho_e\mu_e}\frac{\mathrm{d}}{\mathrm{d}x}\left(\rho_e\mu_e\right)\right],\quad m_2=\frac{x}{u_e}\frac{\mathrm{d}u_e}{\mathrm{d}x},\\ b=\frac{\rho\mu}{\rho_e\mu_e},\quad c=\frac{\rho_e}{\rho},\quad d=\frac{bu_e^2}{H_e}\left(1-\frac{1}{Pr}\right),\quad e=\frac{b}{Pr},\end{gathered} \tag{13}$$

where prime denotes partial differentiation in respect to η, ($f'=\frac{\partial f}{\partial \eta}$). The boundary conditions are now transformed to (classical BL formulation),

$$\begin{aligned}&\eta=0: \quad f=f'=0,\quad S=S_w,\\ &\eta=\eta_e: \quad f'=1,\quad S=1.\end{aligned} \tag{14}$$

In this study, we use the previously obtained data as initial flow distributions. We have developed a two-dimensional computational program where we can obtain the flow field until the separation point, $x = x_s$, [17]. The specified flow field has to be consistent with the classical BL formulation or has to be obtained from experimental data of an actual flow field. Non-physical disturbances and oscillations may appear in the numerical solutions if the flow field is not chosen appropriately [25].

3. Numerical Solution of the Problem

To study the bubble formation after laminar flow separation, a numerical scheme must be applied. The scheme utilized to solve the inversed problem, Equations (7)-(9), is a version of the Keller-box method [17] [18] [20] [26]. The scheme is unconditionally stable, and second-order accuracy is achieved with nonuniform x and η spacing [27]. The equations are written as a first-order system and the derivatives of the unknown function $f(x, \eta)$, with respect to η are introduced as new functions. Further, using central-difference derivatives for the unknown functions at the midpoints of the net rectangle, the obtained difference equations are nonlinear and implicit. The numerical scheme is then applied to the first-order equations. This provides a block tridiagonal system, which is solved by the block elimination method. Since the difference equations are nonlinear the Newton method is used [17].

To describe the presence of an adverse pressure gradient (in the forward problem—classical formulation) we consider, as an example, the linearly retarded flow, known as Howarth's flow, in which the external velocity (at the edge of the boundary layer) varies linearly with x, as shown in the following equation [17],

$$u_e(\bar{x}) = u_\infty(1-\bar{x}), \tag{15}$$

where u_∞ is the free-stream velocity and $\bar{x} = x/L$, L is the length of the boundary surface. The basis pressure is the atmospheric pressure, approx. 1 atm ≈ 101,374.14 Pa. All performed simulations of this study used this pressure as a basis. The free-stream and BL edge values, such as μ_e, ρ_e, were calculated from formulas, e.g., the viscosity, μ_∞, is calculated using Sutherland's law [17]. In this work, we assume that the fluid is air (perfect gas), at about T_∞ = 300 K, with Prandtl number, Pr = 0.708. More details can be found elsewhere [17] [20] [28].

Reverse Flow and Downstream—Upstream Iterations

When the flow is about to reverse, we utilize the Reyhner-Flugge-Lotz (RFL) approximation, as described in [25]. This approximation is dropping the term, uu_x, in the x-momentum equation when the u-velocity becomes negative. We use an iterative procedure to correct the RFL approximation. The downstream pass of the iteration solves the inverse problem described in the previous section, Equations (7)-(9). After any downstream pass we employ an upstream one [25]. This computation is confined to the reverse flow region. The whole idea was initially introduced in the BL theory by Klemp and Acrivos [29].

The numerical code was tested for grid independence and a Table is presented below, **Table 1** [28]. The numerical results for separation point, x_s (m) and maximum temperature, $T_{\max}$ (K), for different configurations of the grid are shown. The results are presented for three Mach numbers, M = 0.2, 0.33 and 1.0, the flow is adiabatic and laminar, the free stream temperature is T_∞ = 300 K. The numerical solution for the first level of calculations (classical boundary layer formulation) is obtained when the difference of the dimensionless skin friction

Table 1. Grid independence data of the computational approach.

Grid size	Mach num, M = 0.2 x_s, $T_{\max}$		Grid size	Mach num, M = 0.33 x_s, $T_{\max}$		Grid size	Mach num, M = 1.0 x_s, $T_{\max}$	
97 × 110 = 10670	0.9588,	300.613	97 × 110 = 10670	0.9588,	301.665	91 × 110 = 10010	0.8989,	314.273
145 × 110 = 15950	0.9592,	300.614	144 × 110 = 15840	0.9525,	301.662	136 × 110 = 14960	0.8993,	314.322
193 × 110 = 21230	0.9594,	300.615	192 × 110 = 21120	0.9544,	301.666	181 × 110 = 19910	0.8994,	314.351

coefficient, f''_w, is less than 10^{-5}, [17]. We have formulated a variable computational grid. This grid is very dense close to the wall and becomes coarser as we move away the wall, to capture all near wall action, **Figure 2**. The developed numerical approach has been validated for laminar and turbulent flows [3] [30]. A validation of this code and the mathematical model with analytical approximate solutions is presented in [30].

For the solution of the inverse problem a computational program was developed in Matlab (MathWorks, Natick, MA, USA). We use the Levenberg-Marquardt algorithm for the solution of the obtained non-linear algebraic problem. The residual error of the algorithm for the inverse problem is of the order of 10^{-8}.

4. Results and Discussion

In this section, we present preliminary numerical results of the bubble formation for low Mach numbers. We focus the analysis to laminar flow separation and bubble formation of the compressible BL for Mach numbers, $M = 0.2$, 0.33 and 1.0. The local Reynolds number of the presented results close to the point of separation are, $R_x = 3.93 \times 10^6$, 6.46×10^6, 1.87×10^7, for the corresponding Mach numbers. Initially, we evaluate the BL before the separation point and these numerical solutions are based on the classical BL formulation. In the next subsection, we present the BL formation for the case of an adiabatic wall [17].

4.1. Results until Separation Point for Laminar Boundary Layer

In this subsection, we present the data obtained from the classical BL formulation,

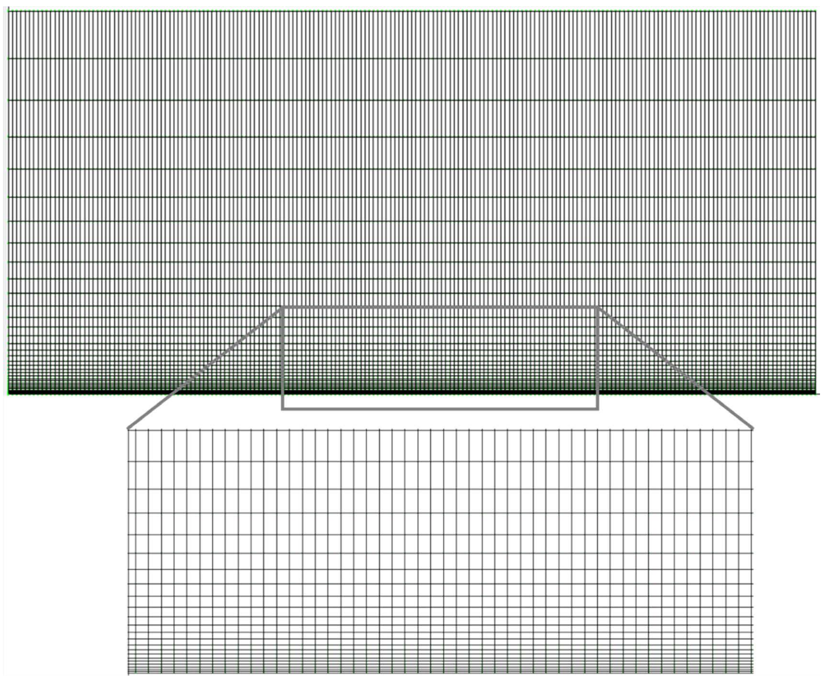

Figure 2. The computational grid for the BL and a zoomed area close to the wall. We have formulated a variable computational grid where is very dense close to the wall and becomes coarser as we move away the wall, to capture all near wall action.

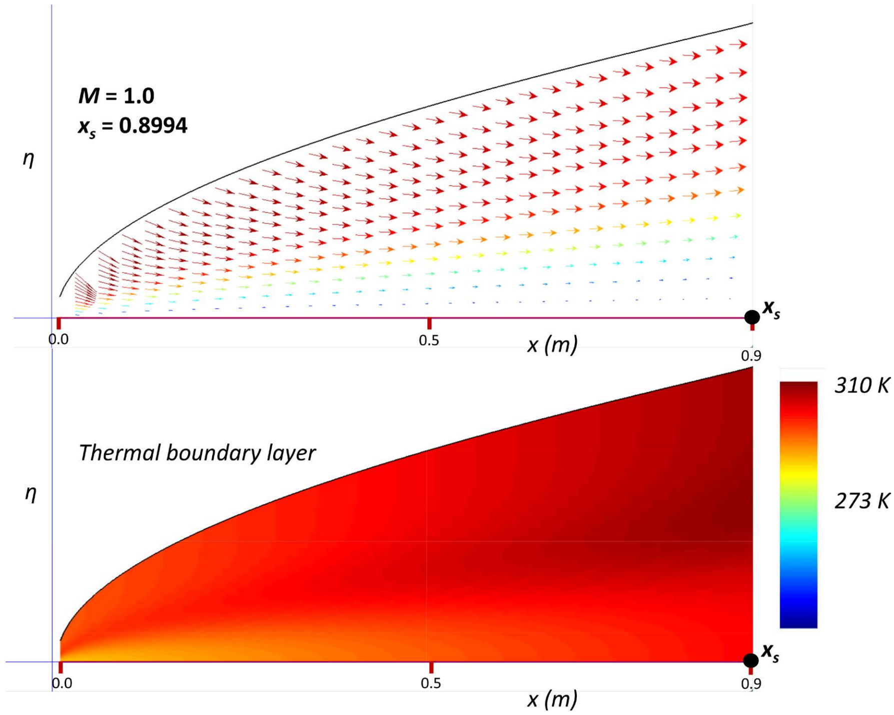

Figure 3. Velocity vectors and temperature distribution of the laminar BL for Mach number, $M = 1.0$, location of separation from the leading edge, $x_s = 0.8994$ m.

as initial data, for calculating the laminar bubble formation for different Mach numbers. **Figure 3** reveals the laminar BL for Mach number, $M = 1.0$, under adverse pressure gradient and for the case of an adiabatic wall, until the location of flow separation, $x = x_s$, [17]. It is observed that for this Mach number the laminar BL separates at the location, $x_s = 0.8994$ m, from the leading edge of the flat plate. In this figure, we also present the thermal BL that follows the laminar BL, showing a small temperature increase from the initial free stream temperature, $T_\infty = 300$ K.

Additionally, **Figure 4** presents the skin friction coefficient, C_{fx}, for the three studied cases, $M = 0.2$, 0.33 and 1.0, under adverse pressure gradient [17] [18]. The skin friction coefficient initially has a large value and reduces as x increases, until it becomes zero, revealing the location of flow separation. The figure reveals the point of separation for each case. So, in detail and for Mach number $M = 0.2$ the flow separates at $x_s = 0.9594$ m, from the leading edge of the flat plate. For the other two cases, $M = 0.33$ and 1.0 the separation point is $x_s = 0.9544$ and 0.8994 m, respectively. These data are used for the calculation of the laminar bubble formation discussed in the next subsection.

4.2. Results on the Bubble Formation

In this subsection, we present the numerical data obtained from the mathematical description of the laminar bubble formulation (inverse problem) for three different Mach numbers. The numerical results of bubble formation in low Reynolds numbers reveal that after separation a laminar bubble is formed in all

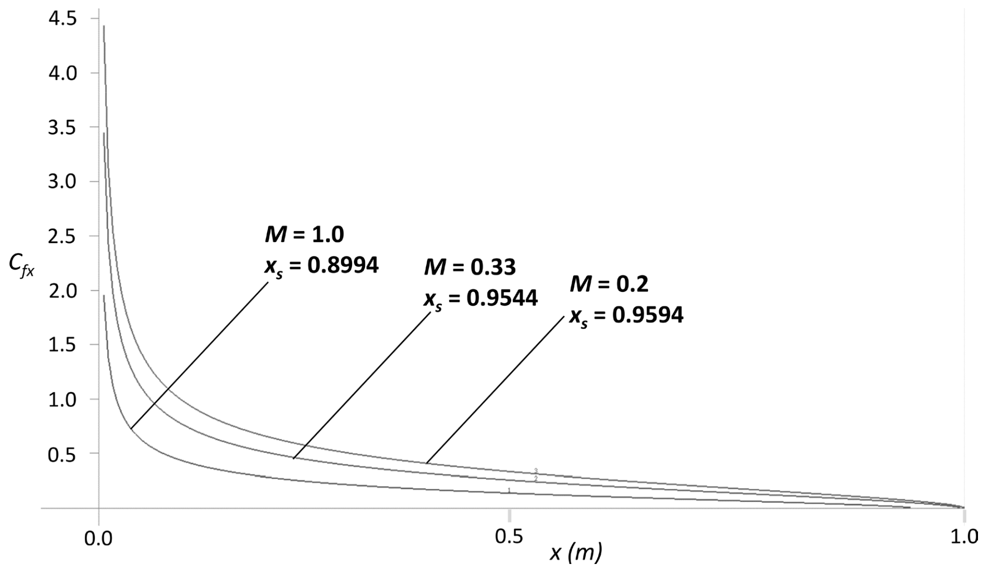

Figure 4. Skin friction coefficient, C_{fx}, of the laminar boundary layer for Mach numbers, $M = 0.2$, 0.33 and 1.0 and corresponding separation locations, x_s.

studied cases, Mach numbers, $M = 0.2$, 0.33 and 1.0. The flow after separation reverses close to the wall and finally reattaches in the x-direction, as depicted in **Figure 5**. As the Mach number increases, this effect is more intense. More precisely, for the case where $M = 0.2$, a small recirculation region is observed close to the wall. The velocity is substantially reduced. After reattachment the BL is again established but in a much lower energy level and the velocity field is substantially reduced, compared to the initial flow field. The BL, due to the adverse pressure gradient, moves upward as shown in **Figure 5**. The same behavior is obtained for the other two Mach numbers, $M = 0.33$ and 1.0. The bubble formation is more pronounced for the larger Mach number, $M = 1.0$. In this case, the velocity after separation is also increased compared to the other two cases.

Advantages and disadvantages of the obtained results. The preliminary results show that the presented approach can effectively describe the flow after separation (laminar bubble formation). This approach is novel and promising, since the fact that until recently scientists believed that BL mathematical theory was not sufficient to describe separated flows and regions of reverse flow. Comparing these results with previous studies, in a qualitative way, we observe that these data are well related with previous numerical approaches [25]. After separation usually the reattached BL is transient or fully turbulent. This study cannot capture the turbulent flow after reattachment since mathematically describes the laminar bubble formation. A more detailed comparison of the numerical results with experimental data should be performed in a future study.

Mathematical description of flow separation and bubble formation is a key element in the field of aerodynamics. Nowadays, with the strides achieved in mathematical modeling, numerical analysis, and computers we can describe such phenomena providing vital information about the aerodynamic performance of the device.

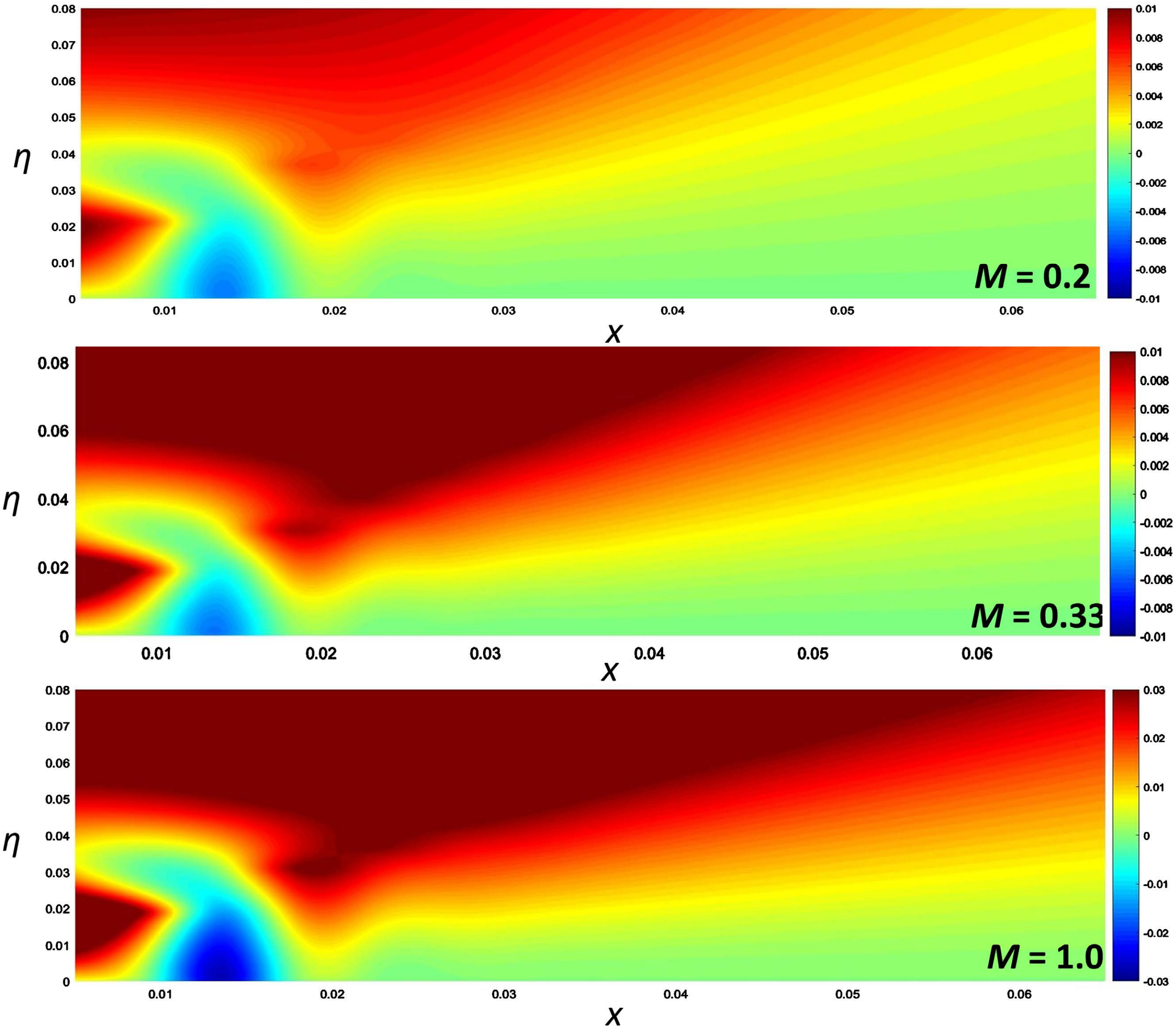

Figure 5. Velocity contours of bubble formation after separation for various Mach numbers, M = 0.2, 0.33 and 1.0.

5. Conclusions and Future Steps

At low Mach and Reynolds numbers, fluid devices are strongly influenced by the formation of laminar separation bubbles. Such a laminar separation bubble is usually caused by a strong adverse pressure gradient along the surface, leading to the separation of the BL from the flat surface. Presence of these bubbles has an undesired and weakening effect on the performance of the fluid device. The understanding of the prevailing mechanism of the separation bubble and ways to control it are essential for the efficient design of these devices.

The study introduces a two-dimensional mathematical formulation of bubble formation after flow separation. The laminar BL equations with appropriate boundary conditions are dimensionalized using the Falkner-Skan transformation. The Keller-box method is used to numerically solve the nonlinear system of PDEs. The presented formulation (inverse formulation) is different from the classical boundary layer formulation and can effectively evaluate bubble formation occurring after the separation point. To obtain the flow field before separation, we utilize the data from the numerical code developed in our previous studies [17]. This code is based on the classical boundary layer formulation.

The preliminary numerical results of bubble formation in low Reynolds numbers reveal that after separation, a laminar bubble is formed in all studied cases, $M = 0.2$, 0.33 and 1.0. The flow after separation reverses close to the wall and finally reattaches downstream in a new location, at the x-direction. As the Mach number increases, this effect is more intense. After reattachment, the BL is again established but at a much lower energy level and the velocity field is substantially reduced, for all studied cases. The presented approach can effectively describe the flow after separation (laminar bubble formation). This approach is novel and promising, since the fact that until recently scientists believed that BL mathematical theory was not sufficient to describe separated flows and regions of reverse flow. In future steps, additional studies are required for delineating this phenomenon that could have a deteriorating effect on the performance of a fluid device.

Conflicts of Interest

The author declares no conflicts of interest regarding the publication of this paper.

References

[1] Rossow, V.J. (1957) On Flow of Electrically Conducting Fluids over a Flat Plate in the Presence of a Transverse Magnetic Field. NASA Report 1358.

[2] Bleviss, Z.O. (1958) Magnetogasdynamics of Hypersonic Couette Flow. *Journal of Aero/Space Science*, **25**, 601-615. https://doi.org/10.2514/8.7812

[3] Xenos, M. and Pop, I. (2017) Radiation Effect on the Turbulent Compressible Boundary Layer Flow with Adverse Pressure Gradient. *Applied Mathematics and Computation*, **299**, 153-164. https://doi.org/10.1016/j.amc.2016.11.024

[4] Ali, M.M., Chen, T.S. and Armaly, B.F. (1984) Natural Convection-Radiation Interaction in Boundary-Layer Flow over Horizontal Surfaces. *AIAA Journal*, **22**, 1797-1803. https://doi.org/10.2514/3.8854

[5] Raptis, A. and Toki, C.J. (2009) Thermal Radiation in the Presence of Free Convective Flow past a Moving Vertical Porous Plate: An Analytical Solution. *International Journal of Applied Mechanics and Engineering*, **14**, 1115-1126.

[6] Raptis, A. and Perdikis, C. (2003) Thermal Radiation of an Optically Thin Gray Gas. *International Journal of Applied Mechanics and Engineering*, **8**, 131-134.

[7] Anghaie, S. and Chen, G. (1998) Application of Computational Fluid Dynamics for Thermal Analysis of High Temperature Gas Cooled and Gaseous Core Reactors. *Nuclear Science and Engineering*, **130**, 361-373. https://doi.org/10.13182/NSE98-A2012

[8] Duan, L., Martin, M.P., Sohn, I., Levin, D.A. and Modest, M.F. (2011) Study of Emission Turbulence-Radiation Interaction in Hypersonic Boundary Layers. *AIAA Journal*, **49**, 340-348. https://doi.org/10.2514/1.J050508

[9] Duan, L., Martin, M.P., Feldick, A.M., Modest, M.F. and Levin, D.A. (2012) Study of Turbulence-Radiation Interaction in Hypersonic Turbulent Boundary Layers. *AIAA Journal*, **50**, 447-453. https://doi.org/10.2514/1.J051247

[10] Miroshnichenko, I.V. and Sheremet, M.A. (2015) Numerical Simulation of Turbulent Natural Convection Combined with Surface Thermal Radiation in a Square Cavity. *International Journal of Numerical Methods for Heat & Fluid Flow*, **25**, 1600-1618. https://doi.org/10.1108/HFF-09-2014-0289

[11] Miroshnichenko, I.V., Sheremet, M.A. and Mohamad, A.A. (2016) Numerical Simulation of a Conjugate Turbulent Natural Convection Combined with Surface Thermal Radiation in an Enclosure with a Heat Source. *International Journal of Thermal Sciences*, **109**, 172-181. https://doi.org/10.1016/j.ijthermalsci.2016.06.008

[12] Kim, S.S. and Baek, S.W. (1996) Radiation Affected Compressible Turbulent Flow over a Backward Facing Step. *International Journal of Heat and Mass Transfer*, **39**, 3325-3332. https://doi.org/10.1016/0017-9310(96)00046-4

[13] Türkyılmazoglu, M., Gajjar, J.S.B. and Ruban, A. (1999) The Absolute Instability of Thin Wakes in an Incompressible/Compressible Fluid. *Theoretical and Computational Fluid Dynamics*, **13**, 91-114. https://doi.org/10.1007/s001620050006

[14] Türkyilmazoglu, M. (2002) The Absolute Instability of Joukowski-Type Airfoils. *Theoretical and Computational Fluid Dynamics*, **15**, 255-264. https://doi.org/10.1007/s001620100053

[15] Türkyilmazoglu, M. (2002) Flow in the Vicinity of the Trailing Edge of Joukowski-Type Profiles. *Proceedings of the Royal Society of London. Series A*, **458**, 1653-1672. https://doi.org/10.1098/rspa.2001.0942

[16] Achala, N.L. and Sathyanarayana, S.B. (2015) Approximate Analytical Solution of Compressible Boundary Layer Flow with an Adverse Pressure Gradient by Homotopy Analysis Method. *Theoretical Mathematics & Applications*, **5**, 15-31.

[17] Kafoussias, N., Karabis, A. and Xenos, M. (1999) Numerical Study of Two-Dimensional Laminar Boundary Layer Compressible Flow with Pressure Gradient and Heat and Mass Transfer. *International Journal of Engineering Science*, **37**, 1795-1812. https://doi.org/10.1016/S0020-7225(99)00002-6

[18] Kafoussias, N.G. and Xenos, M.A. (2000) Numerical Investigation of Two-Dimensional Turbulent Boundary-Layer Compressible Flow with Adverse Pressure Gradient and Heat and Mass Transfer. *Acta Mechanica*, **141**, 201-223. https://doi.org/10.1007/BF01268678

[19] Xenos, M., Kafoussias, N. and Karahalios, G. (2001) Magnetohydrodynamic Compressible Laminar Boundary Layer Adiabatic Flow with Adverse Pressure Gradient and Continuous or Localized Mass Transfer. *Canadian Journal of Physics*, **79**, 1247-1263. https://doi.org/10.1139/p01-067

[20] Cebeci, T. and Bradshaw, P. (1984) Physical and Computational Aspects of Convective Heat Transfer. Springer-Verlag, New York. https://doi.org/10.1007/978-3-662-02411-9

[21] Diwan, S.S. and Ramesh, C. (2007) Laminar Separation Bubbles: Dynamics and Control. *Sadhana*, **32**, 103-109. https://doi.org/10.1007/s12046-007-0009-7

[22] O'Meara, M.M. and Mueller, T.J. (1987) Laminar Separation Bubble Characteristics on an Airfoil at Low Reynolds Numbers. *AIAA Journal*, **25**, 1033-1041. https://doi.org/10.2514/3.9739

[23] Malkiel, E. and Mayle, R.E. (1996) Transition in a Separation Bubble. *Journal of Turbomachinery*, **118**, 752-759. https://doi.org/10.1115/1.2840931

[24] Bragg, M.B. and Gregorek, G.M. (1987) Experimental Study of Airfoil Performance

with Vortex Generators. *Journal of Aircraft*, **24**, 305-309. https://doi.org/10.2514/3.45445

[25] Cebeci, T., Keller, H.B. and Williams, P.G. (1979) Separating Boundary-Layer Flow Calculations. *Journal of Computational Physics*, **31**, 363-378. https://doi.org/10.1016/0021-9991(79)90052-4

[26] Cebeci, T. and Smith, A.M.O. (1974) Analysis of Turbulent Boundary Layers. Academic Press, New York.

[27] Keller, H.B. (1970) A New Difference Scheme for Parabolic Problems. In: Bramble, J., Ed., *Numerical Solutions of Partial Differential Equations*, *II*, Academic Press, New York, 327-350.

[28] Xenos, M., Dimas, S. and Kafoussias, N. (2005) MHD Compressible Turbulent Boundary-Layer Flow with Adverse Pressure Gradient. *Acta Mechanica*, **177**, 171-190. https://doi.org/10.1007/s00707-005-0221-7

[29] Klemp, J.B. and Acrivos, A. (1972) A Method for Integrating the Boundary-Layer Equations through a Region of Reverse Flow. *Journal of Fluid Mechanics*, **53**, 177-191. https://doi.org/10.1017/S0022112072000096

[30] Xenos, M.A., Petropoulou, E.N., Siokis, A. and Mahabaleshwar, U.S. (2020) Solving the Nonlinear Boundary Layer Flow Equations with Pressure Gradient and Radiation. *Symmetry*, **12**, Article No. 710. https://doi.org/10.3390/sym12050710

Appendix

Figure A1 shows the velocity contours after separation and the dimensionless

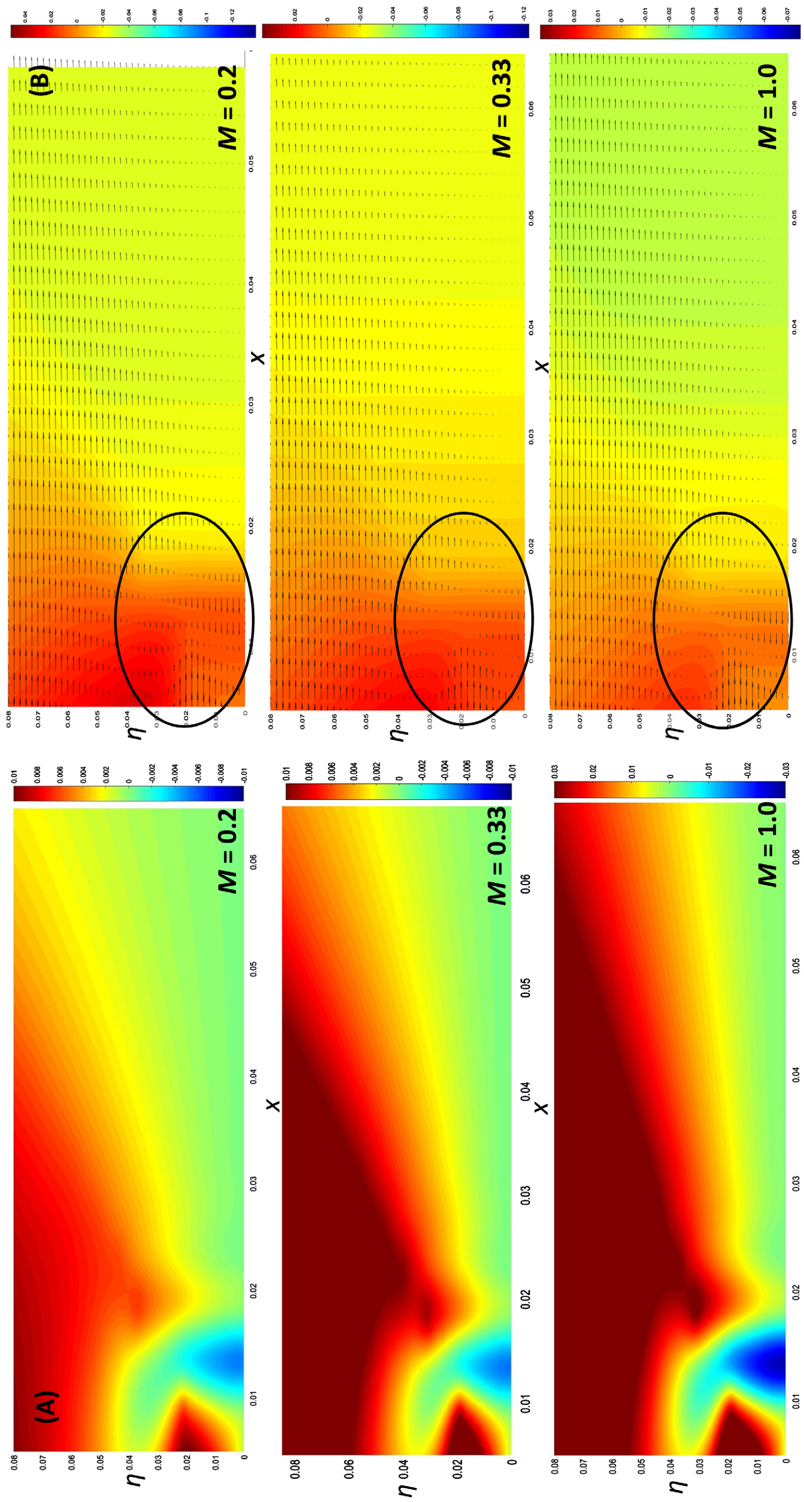

Figure A1. (A) Velocity contours of bubble formation after separation for various Mach numbers, $M = 0.2$, 0.33 and 1.0. (B) Dimensionless stream function and the arrows of velocity for the same Mach numbers. The circle indicates the bubble formation.

stream function in combination with the arrows of velocity, for various Mach numbers. As depicted in Figure A1(B), there is a drastic drop in the stream function after separation revealing that the BL undergoes a dramatic effect. The BL has experienced intense energy losses and the velocity reduces substantially after separation, Figure A1(A). So, there is a sharp change for the stream function after the bubble formation for all Mach numbers of this study, $M = 0.2$, 0.33 and 1.0. Additionally, we plot the velocity field that captures flow separation and the bubble formation, Figure A1(B). We mark with a circle the location of bubble formation. It can be observed that the bubble, in all three studied cases, is small and the BL eventually overcomes the bubble formation, Figure A1.

We further present the qualitative bubble formation in one of the studied cases, for Mach number, $M = 0.33$. In Figure A2, we focus the attention at the recirculation zone as to visualize the bubble construction. We highlight the bubble region with a blue solid line.

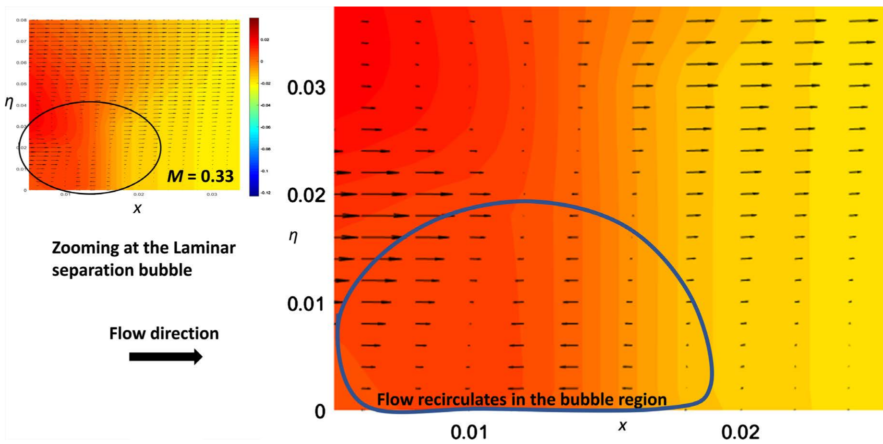

Figure A2. Focusing the attention at the recirculation zone, we highlight the bubble formation region with the blue solid line for the case of $M = 0.33$.